Materials Physics and Mechanics 38 (2018) 54-63 Received: March 16, 2018

MICROSTRUCTURE EVOLUTION OF A TI/TIB METAL-MATRIX COMPOSITE DURING HIGH-TEMPERATURE DEFORMATION

M.S. Ozerov, M.V. Klimova, N.D. Stepanov, S.V. Zherebtsov*

Laboratory of Bulk Nanostructured Materials, Belgorod State University, Belgorod, Russia

*e-mail: zherebtsov@bsu.edu.ru

Abstract. A Ti/TiB metal-matrix composite (MMC) was produced by spark plasma sintering using a Ti-10wt.%TiB_2 powder mixture at 850°C under a load of 40 MPa for 15 min. The microstructure evolution and mechanical behavior of the Ti/TiB composite during uniaxial compression at the temperature range 500 - 1050°C was studied. The evolution of microstructure of the titanium matrix was associated with the formation of dislocation cells at 500°C, continuous dynamic recrystallization at 700°C and discontinuous dynamic recrystallization at temperatures ≥ 850°C. The apparent activation energy of the deformation and processing map were analyzed. The contributions of different strengthening mechanisms of the composite were evaluated.

Keywords: metal-matrix composite; spark plasma sintering; uniaxial compression; dynamic recrystallization; activation energy; precipitation hardening.

1. Introduction

Titanium and its alloys are attractive for applications in various industries due to its encouraging properties (high specific strength, corrosion resistance). However, practical usage of titanium alloys is often limited by their insufficient strength, hardness, and wear resistance. One of the solutions to this problem is creating composites based on titanium, using a reinforcing high-strength component. In this case, the high strength of the reinforcing component is combined with the high toughness of the titanium matrix.

Among the various reinforcements, TiB is the most attractive because it has a density close to that of titanium, a high Young modulus, creates minimal residual stresses due to a close coefficient of thermal expansion, and also has good crystallographic interphases with a titanium matrix [1-3].

During synthesis of the Ti/TiB composite by spark plasma sintering (SPS) process, the TiB phase is formed as a result of the chemical reaction $Ti + TiB_2 \rightarrow Ti + 2TiB$ [1, 3]. This method has certain advantages: high synthesis speed helps to preserve the high dispersity of the original powders; besides, it is possible to achieve almost 100% density of the specimens [4, 5].

Meanwhile, the presence of the TiB hardening phase not only increases the strength but also significantly reduces the plasticity of the composite. The possibility of increasing ductility of a titanium alloy reinforced with TiB fibers due to high-temperature 2D deformation was shown in [7]. Unfortunately, this is a limited number of thorough investigations of the microstructure evolution during thermomechanical processing [8]. Therefore, additional studies of different temperature-rate conditions of thermomechanical processing on the structure and mechanical properties of the Ti/TiB composite are required.

http://dx.doi.org/10.18720/MPM.3812018_8

2. Materials and methods

To synthesize the Ti/TiB composite, titanium powder (99.1% purity) with an average particle size of 25±10 μm and titanium diboride TiB_2 powder (99.9% purity) with a mean particle size of 4.0±1.5 μm were used. The weight fraction of TiB_2 in the initial mixture was 10%, which corresponded to 17 vol. % TiB after synthesis [10]. The selected amount of reinforcing component provides practically the maximum strengthening effect, further increase of TiB_2 in the initial mixture does not give an appreciable increase in strength, but leads to a sharp drop in ductility [1]. A mixture of Ti powder with 10 wt. % of TiB_2 was prepared using a Retsch RS200 vibrating cup mill for 1 h in ethanol at the milling rotation speed of 700 rpm. The grinding set was cooled with liquid nitrogen (T=-196°C) to prevent heating of the mixture during mixing. The spark plasma sintering process was carried out using the Thermal Technology SPS10-3 unit at a temperature of 850°C at a pressure of 40 MPa and a holding time of 5 minutes. Specimens ∅19×15 mm were obtained. The temperature of the polymorphic transformation of the titanium matrix of the composite was ~915°C.

Samples ∅7×10 mm were cut from composite blanks using the electro-erosion machine Sodick AQ300L. Specimens were compressed isothermally in air at 500, 700 or 850°C (α phase field) and 950, 1000 or 1050°C (β phase field) with an Instron mechanical testing machine at a nominal strain rate of 10^{-3} s^{-1} to a true strain ε ≈1.2 (corresponding to a 70% reduction). The holding time of the specimen at the desired temperature before the start of deformation was 15 minutes. Immediately after stopping the deformation, the sample was removed from the furnace and cooled on air.

Strain-rate jump compressive tests were conducted at temperatures of 800, 850, 950, 1000 and 1050°C and at strain rates of 10^{-2}, 5×10^{-3}, 10^{-3} and $5\times10^{-4}s^{-1}$. The obtained data were used to determine the activation energy of the plastic deformation of the Ti/TiB composite in accordance with [11-13].

The tensile testing was conducted at temperatures of 20°C, 400°C, 500°C, 600°C, 700°C and an constant strain rate of $10^{-3}s^{-1}$. The tensile samples had the gauge length of 4mm and a rectangular gauge cross-section of 3mm×1.5mm. The specimens were carefully mechanically polished. Elongation to fracture was determined by measurements of spacing between marks designating the gauge length before and after the test.

X-ray diffraction (XRD) analysis was done for the shear plane of specimens using an ARL-Xtra diffractometer with CuKα radiation. Quantitative phase analysis was performed using the Rietveld method [14] with PowderCell software. The microstructure in the axial section was studied using scanning electron microscope (SEM) FEI Quanta 600 FEG microscope and a transmission electron microscope (TEM) JEOL JEM 2100. Etching was carried out with Kroll's reagent (95% H2O, 3% HNO3, 2% HF) for SEM observations.

3. Results and discussion

The initial microstructure. The microstructure of the Ti/TiB composite after sintering at 850°C consisted of three structural components: Ti matrix, TiB whiskers that formed during in situ $Ti + TiB_2 \rightarrow Ti+2TiB$ reaction, and retained TiB_2 particles (Figure 1a). The volume fraction of pores in the structure was 0.5%. The average diameter of TiB whiskers was 36±15 nm. The TEM analysis showed the heterogeneous distribution of TiB whiskers in the titanium matrix (Fig. 1b). The TiB whiskers had an irregular hexagonal shape with the sides the parallel to the (100), $(10\bar{1})$ and (101) planes [8] (the insert in Fig. 1b). Many stacking faults were observed in the (100) plane of the TiB whisker. The fractions of the phases determined by the quantitative X-ray analysis were 74.0% Ti, 15.6% TiB and 10.4% TiB_2.

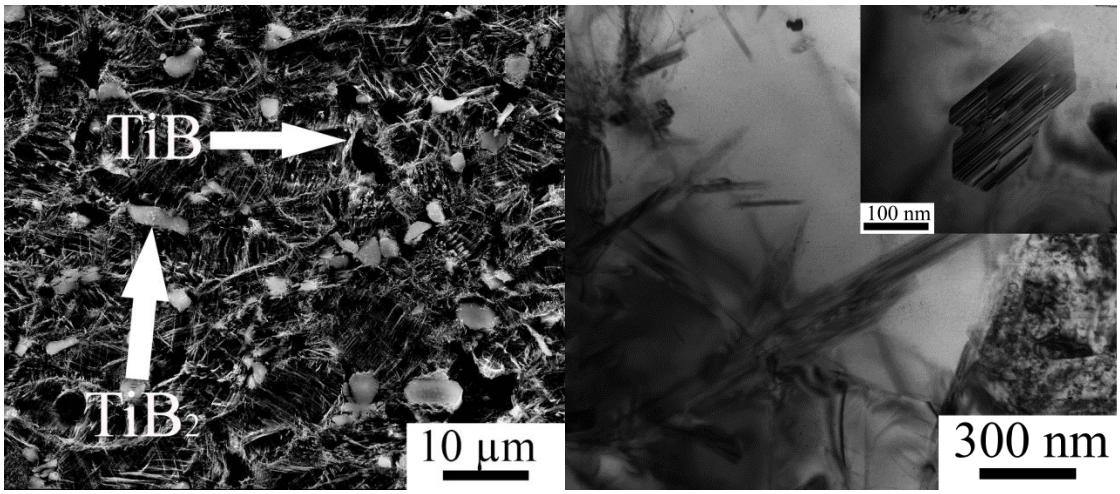

a b

Fig. 1. SEM (a) and TEM (b) images of the Ti/TiB microstructure after SPS at 850°C.

Mechanical properties. The tensile testing of the composite at the temperature range of 400-700°C (Fig. 2) demonstrated appreciable ductility only at temperatures ≥ 500°C. At 400°C the sample was ruptured in the elastic region (corresponding stress-strain curve not presented). It worth noting that the shape of the stress-strain curves obtained at 500-700°C indicated early localization of the plastic flow and a short stage of the uniform deformation. Such deformation behavior is typical of heavily deformed or ultrafine grained metallic materials because of the lack of an effective hardening mechanism [15]. Thus, the obtained results have been showing the possibility of mechanical processing of the Ti/TiB composite at temperatures above 500°C.

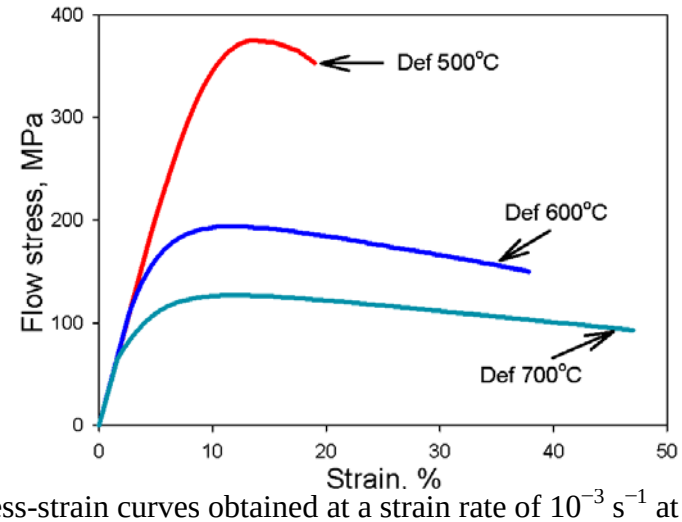

Fig. 2. Tensile stress-strain curves obtained at a strain rate of 10^{-3} s^{-1} at temperatures of 500, 600 and 700°C.

To study the mechanical behavior of the Ti/TiB composite compression tests at temperatures 500-1050°C were carried out. The appearance of the samples after destruction showed the presence of surface cracks up to a temperature of 1050°C (Fig. 3a). The sample compressed at 500°C demonstrated the continuous hardening after the beginning of plastic flow. The stress-strain curves obtained at temperatures of 700-1050°C of the Ti/TiB composite showed the presence of an initial hardening transient, the achievement of a peak flow stress, and then flow softening (Fig. 3h). This behavior can be associated with the processes of dynamic recrystallization or recovery.

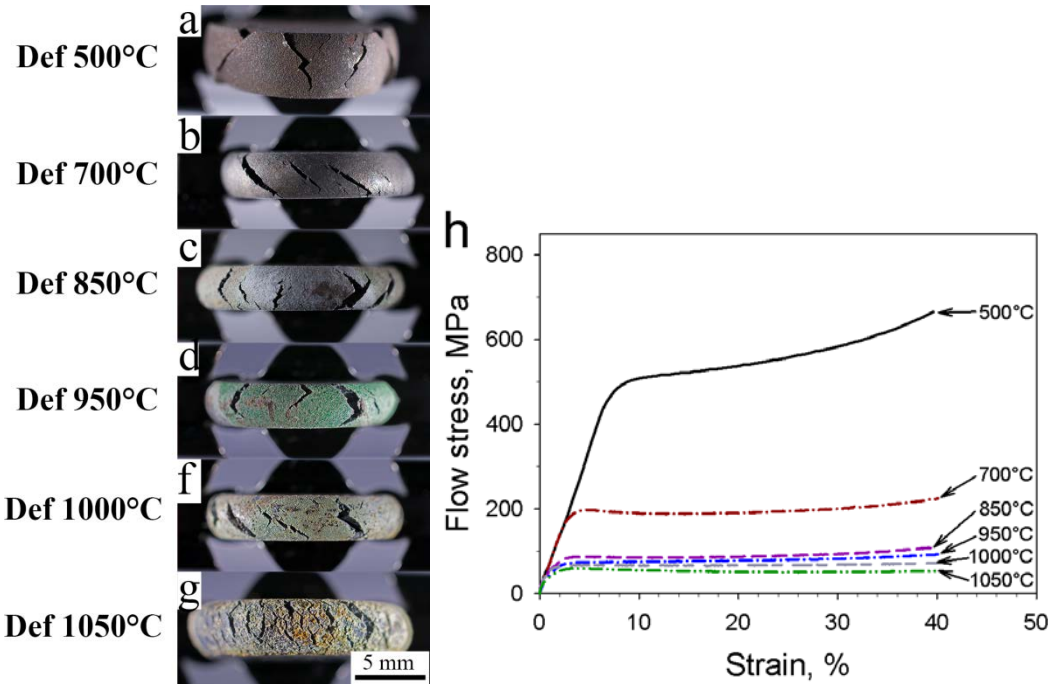

a b

Fig. 3. Specimens of the Ti/TiB composite after isothermal compression at 500 (a), 700 (b), 850 (c), 950 (d), 1000 (e), 1050°C (f) and flow curves obtained during compression at 500-1050 °C and a nominal strain rate of $10^{-3}s^{-1}$ (h).

The microstructure evolution of the Ti/TiB composite during compression tests. The microstructural changes observed in SEM were associated with the rotation of the TiB whiskers in the direction of the plastic flow; the intensity of this process decreases with an increase in the deformation temperature (Fig. 4). Redistribution of the TiB whiskers with the formation of clusters was observed at the deformation temperatures 500-950°C. At higher compression temperatures of 1000-1050°C the TiB whiskers remained rather inhomogeneously distributed in the titanium matrix. A decrease in the fraction of residual TiB_2 is observed with an increase in the deformation temperature.

The TEM investigation showed a more pronounced dependence of the structural changes on the deformation temperature (Fig. 5). The titanium matrix had a typical cellular structure with a high dislocation density after deformation at 500°C (Fig. 5a). The boundaries of the cells were rather wide and loose. The size of the cells varied from a hundred to several hundred nanometers. The interphase Ti/TiB boundaries were blurred due to high internal stresses caused by the high dislocation density. Regions with a size of 1.0-1.5 μm with a low dislocation density, surrounded by rather loose and wide boundaries were observed in the deformed structure after compression at 700°C (Fig. 5b). After deformation at 850°C, grains with a size of ~1 μm with boundaries having a fairly perfect structure with a characteristic banded contrast were found (Fig. 5c). The formation of new grains occurred mainly in regions with a low density of the TiB whiskers. The high density of the TiB particles hindered grain boundary movement thereby preserving deformed microstructure. A completely recrystallized structure with an average grain size of ~ 2.5 μm is observed (Fig. 5d) after compression at 1000°C, corresponding to the β phase field of the titanium matrix.

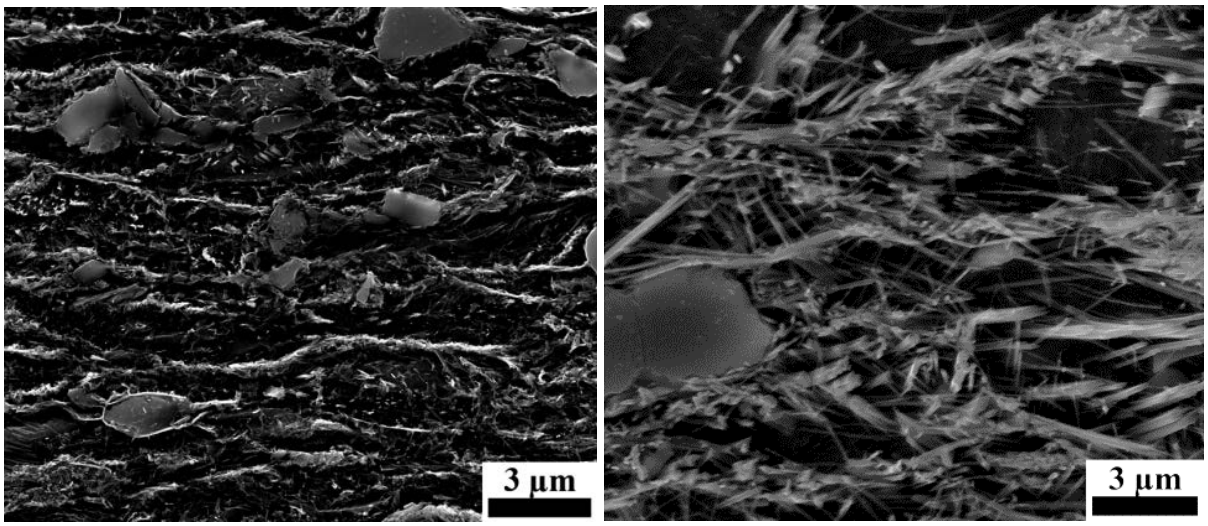

a b

Fig. 4. Microstructure (SEM) of the Ti/TiB composite after compression to 70% at 500 (a) and 1050°C (b).

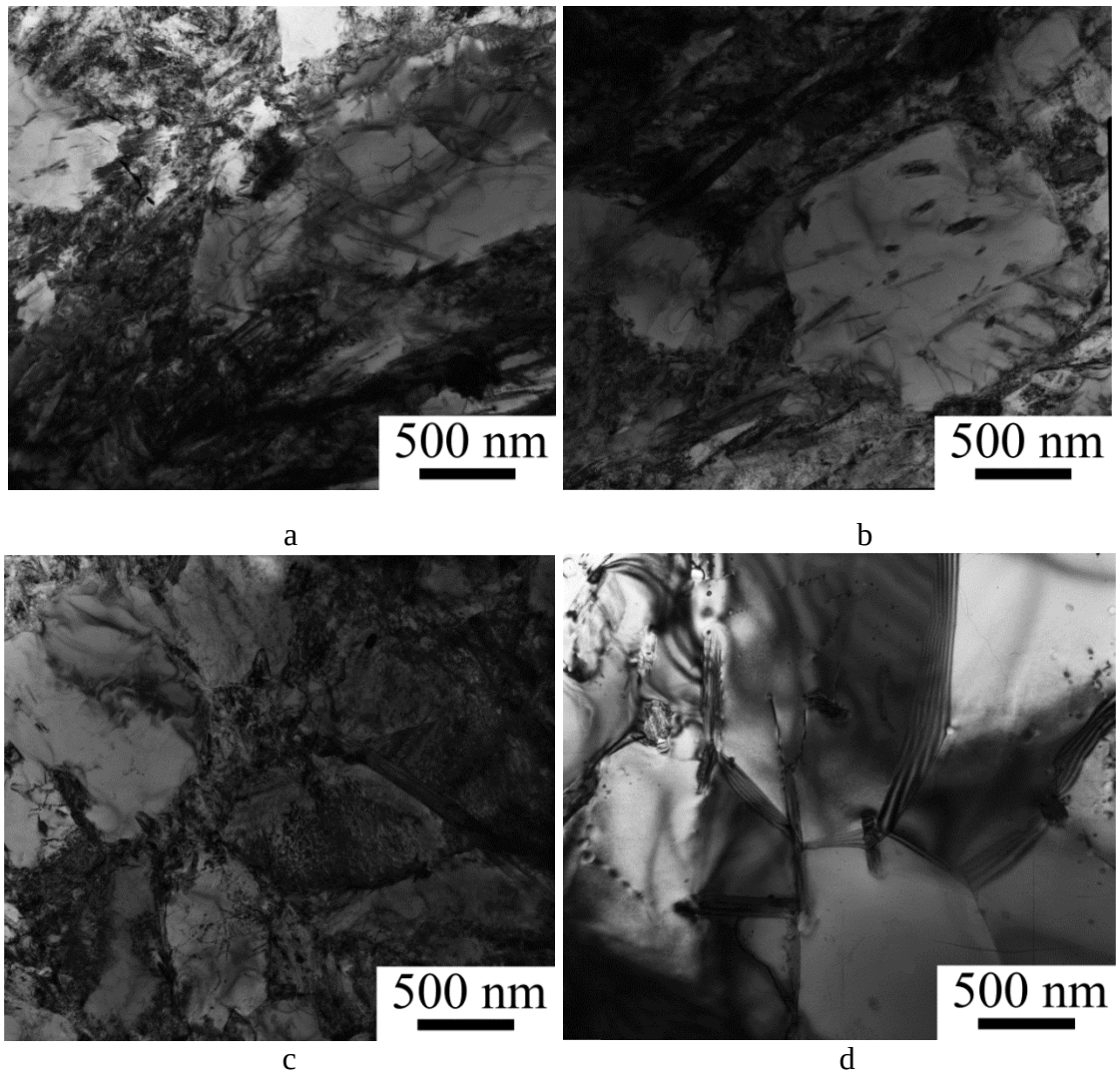

a b

c d

Fig. 5. Microstructure (TEM) of the Ti/TiB composite after compression to 70% at 500 (a), 700 (b), 850 (c) and 1000°C (d).

Quantitative analysis of the TiB whiskers size (Fig. 6) showed a slight change in the transverse dimension (diameter) depending on the deformation temperature in the α field. Some increase in the transverse size of the TiB whiskers (Fig. 6a) was noted after deformation in the β field (T> 900°C) in comparison to the initial state. Probably, it can be associated with a high diffusion rate in the β field. The length of the TiB whiskers sharply (~4 times) decreased as a result of deformation in the α field, and, to a lesser extent (~2.5 times), in the β field. According to [9], the aspect ratio (length to the size of the cross-section) of the TiB whiskers (rather than the diameter) is the main factor which affects the mechanical properties of the titanium-matrix composites. The ratio of length to transverse dimension in the investigated Ti-TiB composite remained constant ~10 (in the initial state ~55) during the deformation.

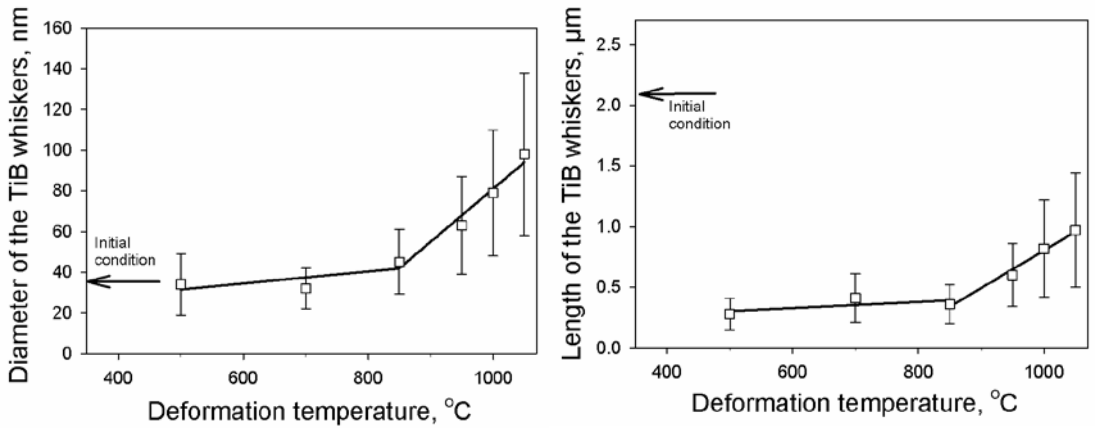

a b

Fig. 6. Change in the transverse dimension (diameter) (a) and length (b) of the TiB whiskers as a result of the Ti/TiB composite`s compression tests at temperatures of 500-1050°C.

Thermoactivation analysis. The results of the analysis of the apparent activation energy of the plastic deformation indicated the presence of three stages (Fig. 7). The value of the activation energy obtained at low deformation temperatures (500-800°C) at a strain rate of $10^{-3}s^{-1}$ and a factor of n=7 was Q=309 kJ/mol. In this temperature range the appearance of partially recrystallized regions and the development of continuous dynamic recrystallization (cDRX) was observed. It is also worth noting that the results obtained are consistent with those given in [16], when the controlling mechanism of deformation is the thermally activated overcoming of the interstitial solute atom obstacles by dislocations. At a deformation temperature of 850°C, the value of the activation energy dropped by ≈ 3 times. This is apparently due to the development of discontinuous dynamic recrystallization (dDRX) and the formation of recrystallized grains. A further increase in the deformation temperature (above 900°C) leads to the activation of new, more energy-intensive processes, providing an increase in the value of the activation energy, which is associated with the α→β phase transition of titanium (~910°C). Some increase in Q values in comparison with the literature data can be due to the development of DRX during deformation [17].

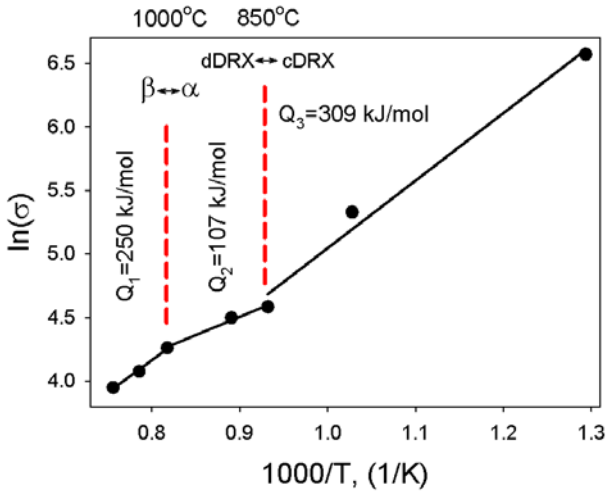

Fig. 7. Arrhenius plot of the logarithmic steady-state flow stress vs the inverse of temperature.

Processing map analysis. The mechanical behavior of metals during hot deformation is often studied to determine optimal temperature-rate parameters for hot working. Processing map analysis reveals areas where the deformation capacity of the material is maximal (for example, the regions of dynamic recrystallization or superplasticity), as well as regions with the unstable plastic flow (for example, the formation of localized shear bands) or with the formation of cracks [18]. For the purpose of such an analysis, a processing map with the strain rate sensitivity of flow stress m (for Ti/TiB m=0.12) was constructed based on the results of mechanical tests. The calculations were made using the following equations:

$$m = \frac{\Delta \log \sigma}{\Delta \log \dot{\varepsilon}}, \quad (1)$$

where σ is the flow stress and $\dot{\varepsilon}$ is the strain rate.

The efficiency of power dissipation (η) of a work piece can be estimated by comparing its power dissipation through microstructural changes with that occurring in an ideal linear dissipator (m = 1) [19]:

$$\eta = \frac{m/(m+1)}{1/2} = \frac{2m}{m+1}. \quad (2)$$

The power dissipation map represents the projection of a three-dimensional surface describing the variation of η with temperature and strain rate on the $T-\dot{\varepsilon}$ plane.

Figure 8 shows a map for the true strain φ=1.2. The map presented a peak with a value of 0.36 in the temperature range of 850°C and low rates of deformation. According to the results of the microstructural analysis, this region corresponded to the development of dDRX (Fig. 5). This result is confirmed by the literature data [18]. The deformation temperature of 850°C is optimal: at lower temperatures extensive formation of cracks occurred (Fig. 3); while at higher deformation temperatures (especially in the β field) the formation of a coarse-grained structure is expected.

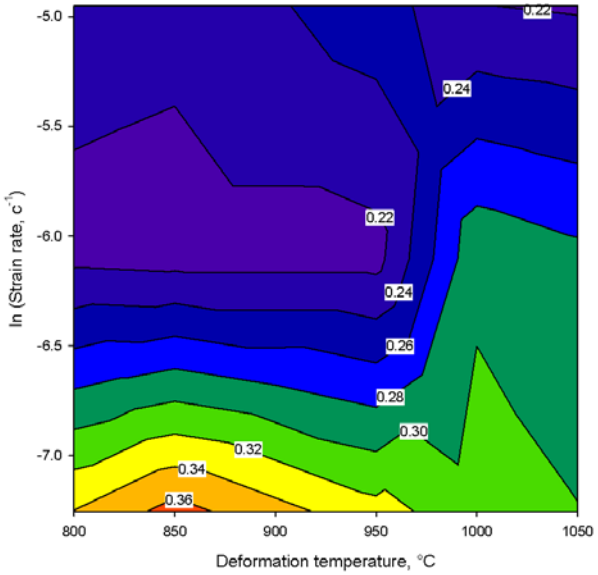

Fig. 8. Processing map of the Ti/TiB composite at a true strain φ=1.2.

Hardening mechanisms. The introduction of the reinforcing TiB component into the ductile titanium matrix, as expected, should change the contribution of the hardening mechanisms during deformation to the resulting value of the composite strength. The contributions of the most relevant hardening mechanisms in hardness of the composite can be expressed as [20, 21]:

$$\sigma_{\Sigma} = \sigma_0 + \sigma_{\rho} + \sigma_{H-P} + \sigma_{L-T} + \sigma_{TiB(OR)}, \quad (3)$$

where σ_0 is the frictional stress including solid-hardening by C, O, N (300 MPa) atoms, σ_{ρ} is the substructure hardening, σ_{H-P} is Hall-Petch hardening, σ_{L-T} is the hardening of the load transfer strengthening effect, $\sigma_{TiB(OR)}$ - the precipitation hardening by the debris of the TiB whiskers (Orowan mechanism).

The substructure hardening can be expressed as [20]:

$$\sigma_{\rho} = M\alpha Gb\sqrt{\rho}, \quad (4)$$

where M is the is the average Taylor factor, α is the constant, G is the shear modulus, b is the Burgers vector, ρ is the dislocation density. For the calculation, the values of M equal to 3 and α equal to 0.5 were taken.

The Hall–Petch contribution to the strength is typically of the form [20]:

$$HV_{H-P} = K_y d^{-1/2}, \quad (5)$$

where K_y is the Hall–Petch coefficient and d is the grain size.

The hardening of the load transfer strengthening effect can be calculated using the formula [21]:

$$\sigma_{L-T} = [\{V_{TiB}\left(\frac{S+2}{2}\right) + V_{Ti}\} - 1], \quad (6)$$

where V_{TiB} and V_{Ti} - the value of the volume fraction of the phase TiB and titanium, S - the parameter of the aspect ratio of the TiB whiskers.

The precipitation hardening by the debris of the TiB whiskers can be expressed as [22]:

$$\sigma_{TiB(OR)} = \frac{MGb}{2.36\pi}\ln\left(\frac{0.57DS^{\frac{1}{3}}}{b}\right)\frac{1}{(0.92V^{-\frac{1}{3}} - 1.14)DS^{\frac{1}{3}}}, \quad (7)$$

where D is the diameter of TiB whiskers, V is the volume fraction of TiB, and S is the aspect ratio of TiB whiskers.

Some input parameters for the titanium matrix were taken from [23]: K_y=0.3 MPa·m$^{1/2}$, σ_0=320 MPa and b=2.9×10^{-10} m. The value of the shear stress G=130 GPa for the Ti/TiB composite was taken from [1].

The ultimate compression strength of the Ti/TiB composite after compression testing at room temperature is 2400 MPa. The theoretical strength calculated by summing the contribution of all the above hardening mechanisms showed a close value of 2200 MPa. The precipitation hardening by the debris of the TiB whiskers makes the most appreciable contribution - 1430 MPa (~ 65%), in [24] a close value was obtained. The hardening due to the load transfer strengthening effect was 220 MPa, the values of the substructure hardening and the Hall–Petch contribution were 140 and 110 MPa, respectively.

4. Conclusions

1) The initial microstructure of the Ti/TiB composite consisted of the TiB whiskers heterogeneously distributed within the Ti matrix. The average diameter of the TiB whiskers was 36 ± 15 nm. The brittle-to-ductile transition temperature of the Ti/TiB composite was 500°C.

2) During the deformation in the temperature range of 500-1050°C the length of the whiskers TiB decreased considerably while the diameter of the whiskers was weakly affected. Thus the aspect ratio of the TiB whiskers decreased from ~55 to ~10 and remains constant up to a deformation temperature of 1050°C. Growth in the diameter and length of the TiB whiskers was observed with an increase in the deformation temperature (above 900°C).

3) The microstructure evolution during the deformation and the apparent activation energy analysis revealed 3 stages: i) 700°C: the controlling mechanism of deformation - continuous dynamic recrystallization - Q=309 kJ/mol; ii) 850-950°C: decrease in Q up to 107 kJ/mol, development of discontinuous dynamic recrystallization; (iii) 1000-1050°C: an increase in the activation energy up to 250 kJ/mol, which is due to the α → β phase transition of titanium (~910°C). An analysis of the deformation map confirmed the development of discontinuous dynamic recrystallization at a deformation temperature of 850°C.

4) Calculations had revealed that the precipitation hardening by the debris of the TiB whiskers provided the biggest contribution to the hardening of the Ti/TiB composite ~65%.

Acknowledgements. *The authors gratefully acknowledge the financial support from the Russian Science Foundation (Grant Number 15-19-00165). The authors are grateful to the personnel of the Joint Research Centre, Belgorod State University for their assistance with the instrumental analysis.*

References

[1] K. Morsi, V.V. Patel // *J. Mater. Sci.* **42** (2007) 2037.
[2] K.S. Ravi Chandran, K.B. Panda, S.S. Sahay // *JOM* **56** (2004) 42.
[3] H. Feng, Y. Zhou, D. Jia, Q. Meng and J. Rao // *Crystal Growth & Design* **7** (2006) 1626.
[4] M. Selva Kumar, P. Chandrasekar, P. Chandramohan, M. Mohanraj // *Mater. Charact.* **73** (2012) 43.
[5] A.V. Ragulya, In: *Encyclopedia of Materials: Science and Technology,* ed. by K.H. Jürgen Buschow et al. (UK, Oxford, 2010), p.1.
[6] M. Ozerov, N. Stepanov, A. Kolesnikov, V. Sokolovsky, S. Zherebtsov // *Materials Letters* **187** (2017) 28.
[7] R.A. Gaisin, V.M. Imayev, R.M. Imayev and E.R. Gaisina // *Russian Physics Journal* **58** (2015) 848.
[8] M. Ozerov, M. Klimova, A. Kolesnikov, N. Stepanov, S. Zherebtsov // *Materials and Design* **112** (2016) 17.

[9] M.Y. Koo, J.S. Park, M.K. Park, K.T. Kim and S.H. Hong // *Scripta Materialia* **66** (2012) 487.
[10] L.J. Huang, L. Geng, B. Wang, L.Z. Wu // *Mater. Design* **45** (2013) 532.
[11] C.M. Sellars // *Phil. Trans. R. Soc. London A* **288** (1978) 147.
[12] T. Sakai, J.J. Jonas // *Acta Metall.* **32** (1984) 189.
[13] T. Sakai, A. Belyakov, R. Kaibyshev, H. Miura, J.J. Jonas // *Prog. Mater. Sci.* **60** (2014) 130.
[14] G. Will, *Powder Diffraction: The Rietveld Method and the two-Stage Method to Determine and Refine Crystal Structures from Powder Diffraction* (Springer, G., 2006).
[15] S. Zherebtsov, E. Kudryavtsev, S. Kostjuchenko, S. Malysheva, G. Salishchev // *Mater. Sci. Eng. A* **536** (2012) 190.
[16] H. Conrad // *Prog. Mater. Sci.* **26** (1981) 123.
[17] S.V. Raj, T.G. Langdon // *Acta Metall.* **37** (1989) 843.
[18] K.P. Rao, Y.V.R.K. Prasad // *Comprehensive Materials Processing* **3** (2014) 327.
[19] *Hot Working Guide: a Compendium of Processing Maps,* ed. by Y.V.R.K. Prasad, S. Sasidhara (ASM International, Materials Park, OH, 1997).
[20] M.A. Meyers, A. Mishra, D.J. Benson // *Prog. in Mat. Sc.* **51** (2006) 427.
[21] K.S. Munir, Y. Zheng, D. Zhang, J. Lin, Y. Li, C. Wen // *Mater. Sci. Eng. A* **696** (2017) 10.
[22] B. Chen, J. Shen, X. Ye, L. Jia, S. Li, J. Umeda, M. Takahashi, K. Kondoh // *Acta Mater.* **140** (2017) 317.
[23] H.J. Frost, M.F. Ashby, *Deformation-Mechanism Maps* (Pergamon Press, UK, 1982).
[24] S. Zherebtsov, M. Ozerov, N. Stepanov, M. Klimova and Yu. Ivanisenko // *Metals* **7** (2017) 507.